Available online at www.sciencedirect.com

ScienceDirect

Acta Materialia 79 (2014) 351–362

Acta MATERIALIA

www.elsevier.com/locate/actamat

The thermodynamics of hydride precipitation: The importance of entropy, enthalpy and disorder

S.C. Lumley [a,d], R.W. Grimes [a], S.T. Murphy [a], P.A. Burr [a,b], A. Chroneos [a,c], P.R. Chard-Tuckey [d], M.R. Wenman [a,*]

[a] Centre for Nuclear Engineering and Department of Materials, Imperial College London, London SW7 2AZ, UK
[b] Institute of Materials Engineering, Australian Nuclear Science & Technology Organisation, Menai, New South Wales 2234, Australia
[c] Faculty of Engineering and Computing, Coventry University, 3 Gulson Street, Coventry CV1 2JH, UK
[d] Nuclear Department, Defence Academy, HMS Sultan, Gosport PO12 3BY, UK

Received 4 April 2014; received in revised form 9 July 2014; accepted 10 July 2014

Abstract

The precipitation of zirconium hydrides from Zr solid solution was investigated using first-principles lattice dynamics simulations. These included the temperature-dependent vibrational enthalpy and vibrational entropy combined with the configurational entropy terms. In contrast with previous approaches, it was found that the latent enthalpy alone is not sufficient to fully describe precipitation of hydrides; a full thermodynamic assessment is required. In particular, the vibrational enthalpy of precipitation assists in stabilizing hexagonal close-packed hydrides and is especially important in forming the metastable ζ phase. The configurational entropy change during precipitation favours face-centred cubic hydrides. Given this, at concentrations below 300 ppm H, no hydride precipitation is predicted, suggesting that when hydrides are seen in those materials it is because the local concentration of H is greater than that measured globally. While γ hydride is the most stable phase, it is very close in energy to the δ phase.

Keywords: Zirconium hydride; Thermodynamics; Density functional theory; Precipitation

1. Introduction

Zr alloys are used for fuel cladding and other in-core structures in water-cooled nuclear reactors due to their good mechanical and corrosion properties and low capture cross-section for thermal neutrons. The uptake of H and its precipitation as hydrides in Zr alloys is important in the ongoing development of fuel cladding for water-cooled reactors [1]. At reactor operating temperatures, H is soluble up to around 100 ppm and extremely mobile in α-Zr [2,3,5]. However, if sufficient H is present or if the solubility limit of H in α-Zr is lowered (commonly due to a reduction in temperature during reactor transients [6]), then H will precipitate out, forming zirconium hydrides. The hydrides are brittle and cause component degradation and may lead to failure of the fuel cladding; this is especially likely if they align along the radial direction of the fuel pin due to stress reorientation [1,4]. Recently proposed changes in the regulations for nuclear fuel cladding to limit H uptake [7] and proposals for ever-longer dry storage times [8] make understanding H solubility and hydride precipitation increasingly important for operators and manufacturers alike.

Current understanding suggests that there are five main ways that H can be sequestrated in Zr metal, namely via the formation of four hydrides (ζ, γ, δ and ε), and via solid solution in Zr [9–12]. The structures of these different

* Corresponding author. Tel.: +44 (0)20 7594 6763; fax: +44 (0)20 7594 6729.
E-mail address: m.wenman@imperial.ac.uk (M.R. Wenman).

http://dx.doi.org/10.1016/j.actamat.2014.07.019
1359-6454/

hydrides are shown in Fig. 1. There is a general relationship of decreasing c/a ratio with increasing H content. Of particular interest is that the most commonly observed δ phase is often reported to have a formula of $ZrH_{1.66}$ and a disordered fluorite structure, while simulators often use a simplified ersatz of periodic $ZrH_{1.5}$ [12,13]. The γ hydride has been assumed to be metastable, as it is less readily observed than the δ hydride [14]. However, other investigations have observed the γ hydride at room temperature [15], under both slow cooling [10] and fast cooling regimes [16]. Overall, it appears that the stability and occurrence of these phases is a complex phenomenon, where the H concentration, thermal treatments, alloying additions and stress states all have a part to play in determining which phases are observed [17].

The focus of this study is on modelling hydrides using ab initio atomistic simulation techniques based on density functional theory (DFT). In α-Zr metal, H preferentially occupies tetrahedral sites in the Zr lattice, rather than other sites [12,18,19]. Some works have focused on the octahedral site as the main location for H atom solution; however, such works appear to be in the minority [20,21]. It has been theoretically predicted that the face-centred tetragonal structure of ZrH_2 can have another stable phase for c/a greater than 1 [22,23]. Zhu et al. [13] studied the ordered hydride phases using DFT; they concluded that δ $ZrH_{1.5}$ is thermodynamically less stable than the other phases at high temperature. Zhong and MacDonald, who published previous DFT results combined with new calculations of the γ phase, suggest the γ phase is stable at temperatures below about 523 K [24].

The simulation of hydrides is complicated due to the random distribution of the H atoms in some phases. Although hydrides have been simulated in the past, few studies have attempted to examine hydrides whilst taking into account the disorder. One of the most successfully used techniques for simulating disordered atomic structures is the special quasi-random structures (SQS) method developed by Zunger et al. [25], which has been used to simulate a range of non-stoichiometric materials and structures. It has also recently been applied to this system [26]. In this study SQS techniques are combined with a statistical analysis of a large number of randomly generated cells, in order to examine the impact of disorder on hydride precipitation. Phonon calculations are also used to calculate thermodynamic properties such as the vibrational entropy and the sensible enthalpy changes during precipitation. Previous studies on other systems by DFT have shown the importance of vibrational entropy on the solubility limit in precipitation reactions from solid solution, and its importance in creating a temperature-dependent understanding of hydride precipitation [27,28]. Thus, a comprehensive view of the enthalpy and entropic contributions towards hydride precipitation in Zr is developed.

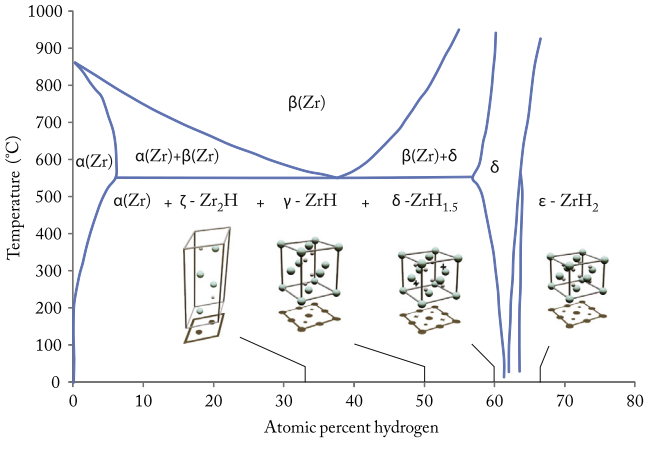

Fig. 1. Structures and formulae of different hydrides found in the Zr–H system. The Zr and H atoms are represented by the larger and smaller spheres, respectively. The δ hydride shown here is as commonly simulated, while real δ phase hydrides have a formula of $ZrH_{1.6}$ and have H atoms arranged randomly across all tetrahedral sites, including the black crosses shown in the diagram. The phase diagram has been reproduced from Ref. [9].

2. Methodology

2.1. Simulation parameters

For this investigation, CASTEP 5.5 was used to simulate the different structures [29]. As a plane-wave pseudopotential code, it is particularly appropriate for modelling crystals. Ultrasoft pseudopotentials were generated "on-the-fly", under the formalisation of Vanderbilt et al. [30].Valence electrons for Zr were modelled as $4s^2 4p^6 5s^2 4d^2$. Convergence with respect to basis-set cut-off energy and k-point grid density was tested in a series of electronic self-consistency calculations. It was found that the simulations were accurate to 2 d.p. for a cut-off energy of 400 eV and a k-point grid spaced of 0.3 nm^{-1}. k-Points were arranged in a gamma-centred Monkhorst–Pack grid [31]. As the system displays metallic characteristics, the integration of the Brillouin zone is achieved via a Methfessel–Paxton scheme, with a band smearing width of 1 eV [32].

All cells used in this work are geometry relaxed in order to approach their minimum energy configuration. Cells were considered relaxed when the difference between two successively modified iterations met all of the following criteria:

- Energy change <0.001 eV.
- Force on ions <0.5 eV nm^{-1}.
- Displacement of ions change <0.01 nm^{-1}.
- Total stress <0.1 GPa.

Relaxation of atomic positions was carried out under the quasi-Newtonian BFGS scheme [33]. Both atomic positions within the cell, the lattice constants and cell aspect ratios were unconstrained during relaxation. This means that volume and cell distortions due to H accommodation are fully accounted for. Previous works [1,34,4] showed that constrained expansion of the hydrides may delay

hydride cracking; however, this is beyond the scope of the current work.

2.2. Thermodynamic considerations

With static simulations it is usual to consider the energy change from a set of reactants to a set of products. Relating the calculated energy changes to a real system is often difficult, as there are numerous different energy components, while static calculations can directly only evaluate the ground state changes (i.e. the latent enthalpy of a reaction). Thus, many factors present in a real system are not represented in a simulation. These different components and factors are often poorly communicated between experimentalists and simulators, leading to inappropriate assumptions when using terms such as energy, enthalpy and entropy. To ensure a clear understanding, the terms that were calculated here are now discussed.

The fundamental measure of the driving force behind a reaction is the Gibbs free energy change:

$$\Delta G = \Delta H - T\Delta S \tag{1}$$

where ΔH represents the enthalpy change of the system and ΔS represents the entropy change. There are different contributors to the enthalpic and entropic terms, thus Eq. (1) can be expanded into:

$$\Delta G(T) = (\Delta H_l + \Delta H_s(T)) - T(\Delta S_v(T) + \Delta S_{cl}) \tag{2}$$

where:

- ΔH_l is the latent enthalpy associated with the reaction. It is due simply to the formation or destruction of bonds and is independent of external conditions. When quoting results from DFT simulations, this is the most commonly reported number. If the other terms are ignored this is often quoted as the energy.
- ΔH_s is the sensible enthalpy and is related to the heat capacities of the different species involved in the reaction. In order to calculate this, the amount of thermal energy that can be stored in the lattice needs to be known. This is achieved by calculating the phonon density of states of the materials in question, and integrating the different acoustic modes in the harmonic approximation, for a temperature T.
- ΔS_v is the vibrational entropy and is a function of the number of discrete vibrational energy levels that exist amongst the different acoustic modes of the system. This is determined by the application of the Boltzmann entropy equation to the harmonic approximation of the phonon distribution [35].
- ΔS_{cl} is the lattice component of the configurational entropy. This only applies to solids with a disordered lattice, which in this system consists of the H sub-lattice. An approximation of this is reported in Section 3.4.

It is clear that the distribution of phonons must be calculated in order to determine two of the terms included here. Analysis of phonon distributions has been previously examined in this system by Blomqvist et al. [23]. In the present study, this was achieved by means of the finite displacement method, in the (direct) supercell approach [36].

In a real precipitation event, there would be stress-related effects, as well as contributions arising from the creation of a hydride–Zr interface. There would also be entropy created by intrinsic defects on the Zr lattice. This study cannot comment on such effects, as they would require simulations that are either significantly larger than the scale that DFT presently allows, or need an exceedingly large number of simulations. However, the numbers produced in this work represent a large portion of the overall driving forces for precipitation, and are a significant advance on what has been achieved for this system previously.

2.3. Cell configurations

This study examines both ordered and disordered models of hydrides and Zr–H solid solutions. The ordered models are performed by a straightforward geometry optimisation of hydride structures including the commonly accepted structures of ζ-Zr_2H, γ-ZrH, δ-$ZrH_{1.5}$ and ε-ZrH_2 [12,11]. In addition, dilute solid solutions were also simulated in which one H atom was placed in $2 \times 2 \times 2$, $3 \times 3 \times 2$ and $4 \times 4 \times 3$ supercells of α-Zr, giving concentrations of 5.8 at.% H, 2.7 at.% H and 1.0 at.% H respectively. A further calculation was carried out in which one H atom was placed in a $2 \times 2 \times 2$ supercell of face-centred cubic (fcc) Zr. All of the solid-solution calculations described so far were carried out with H occupancy being investigated on both octahedral and tetrahedral sites.

A different method was used to simulate more disordered structures. As a starting point for the generation of off-stoichiometric hydride phases, a δ hydride structure is built, formed from a $2 \times 2 \times 2$ supercell of the primitive cell, with all tetrahedral H sites occupied (giving a formula of ZrH_2). This is similar to the ε hydride, except that the c/a ratio is 1. A new cell is generated from this input, by giving each H atom a random chance of being removed of 0.166 (or $1 - \frac{1.6}{2}$). This is repeated to generate a large number of cells, with the only constraint being that new cells must be different to previously generated cells. These cells then undergo geometry optimisation to provide energies for each configuration. No constraints are placed upon the number of H atoms in any given cell, meaning some cells will have more H than the 1.66 ratio, and some will have less. Providing the number of cells is large enough, the formulae of the different cells will follow a normal distribution with a mean of 1.66. A similar method was used with a $2 \times 2 \times 2$ supercell of α-Zr, and a removal probability of 0.89 with single H atom cells discounted. This provides a selection of solid-solution cells where the H exists in small clusters, modally containing two H atoms, which are used to bridge the stoichiometry gap between a dilute solid solution and the ζ phase. These sets will have a number of different possible configurations, which allows examination of how configurationally

sensitive the properties of the hydrides and solid solutions are. Taken together, an arbitrarily large set of these cells provides a more complete description of the δ hydride and a concentrated solid solution than any single periodic calculation. The advantages of random structure generation have been discussed previously [37].

In order to qualify this method against established techniques, the random δ hydride set is compared with SQS-generated cells. The SQS technique, as detailed in Ref. [25], works on the assumption that in any random arrangement of atoms on a predefined set of atomic sites, some clusters of atoms will be more common than others. The more common clusters are defined by the structure and stoichiometry of the simulated crystal. Thus, a number of "special" cells can be constructed that comprise the more common configurations, and less common configurations can be discounted. In this study, three different SQS cells are simulated containing 48, 52 and 56 H atoms, along with 32 Zr atoms. The SQS method has been recently applied to this system in order to model bulk parameters [26]. The three most representative SQS cells in that paper are used again here.

Some phases, however, exhibit more order than the δ phase, such as the γ and ζ phases. Generally, these phases are simulated as ordered phases with a defined structure and no disorder. However, any real hydride will likely exhibit a degree of disorder, particularly when a disordered phase can transform to an ordered phase and vice versa [17]. Thus, a method has been devised to introduce disorder into these structures, whilst biasing the results towards the known structures. In this "skew-random" method, the starting point is a cell of the ordered structure. For each occupied H site, a small removal probability of the H atom is introduced. Likewise, for each unoccupied site, a small chance is created to have a H atom inserted. In both of these cases the probability of 0.05 was used, as it created a reasonable spread of random structures, whilst remaining close to the crystallographic form of the hydride. As before, a large number of these cells were generated and only unique cells are simulated to ensure that the full ensemble of simulations is relevant to a (partially) disordered hydride. A smaller number of random cells was also generated with no structure biasing and a probability of removal of 0.5. These were used purely as a comparison with the skew-random cells.

Ultimately, all possible arrangements of H on interstitial sites in Zr exist as points in the configuration space. Each of the methods described above develops a different sampling of that configuration space, aiming to ensure that a valid distribution is identified.

3. Results

3.1. Elements and ordered crystals

In order to ensure the validity of the simulations performed, the physical and chemical properties of the pure elements in their reference state are presented in Table 1 together with established literature values. Excellent agreement is achieved on all counts, to within a maximum discrepancy of 1.65%.

The enthalpies of formation of different ordered crystals are given in Table 2, following equation:

$$\Delta H_f = \frac{1}{x+y}\left[E(\mathrm{Zr}_x\mathrm{H}_y) - \left(E(x\mathrm{Zr}) + y\frac{1}{2}E(\mathrm{H}_2)\right)\right] \quad (3)$$

where $E(Zr_xH_y)$ represents the energy of the hydride (or solid solution containing H) and the other terms refer to the pure elements. As the number of atoms in each simulation differs, the formation energy must be normalised with respect to the number of atoms, in order not to bias the formation energies towards the larger cells. Solution enthalpies of H atoms in a hexagonal close-packed (hcp) and an fcc matrix are also presented. Although the latter configuration is un-physical (pure fcc Zr is not a stable phase, nor observed in real alloys), it does provide useful comparison points. Although this phase assumes the absorption of H into an fcc lattice, the reference state is still taken to be hcp Zr. This is done to ensure fair comparison with other results and is based on the assumption that any starting point that could lead to this configuration would still be based on hcp Zr. As formation energies for fcc solutions must also contain the energy associated with a hcp $\rightarrow$ fcc phase change, it is reasonable that the formation energies for the fcc solutions are higher than their hcp counterparts. The dilute tetrahedral solid solution is of particular

Table 1
Crystallographic and thermodynamic properties of Zr and H. The bracketed value for α-Zr includes the zero point energy component of atomic vibrations.

	Property	Predicted value	Literature
Zr (hcp)	$a\,(nm)$	0.322	0.323 [53]
	$c\,(nm)$	0.520	0.5145 [53]
	$E_{vaporisation}$ (eV atom^{-1})	6.20 (6.24)	6.24 [42]
Zr (fcc)	$a()$	0.641	–
	$E_f^{fcc} - E_f^{hcp}$ (eV atom^{-1})	0.04	–
H (Gas)	Bond length (pm)	75.2	74.6 [42]
	$E_{disassociation}$ (eV atom^{-1})	4.53	4.52 [42]
	Vibrational frequency (cm^{-1})	4328.42	4401.21 [54]

Table 2
Enthalpies and lattice parameters of ordered crystals.

Structure	at.% H	a (nm)	c (nm)	H_{sol}(eV)	H_f(eV atom^{-1})
hcp-Zr(H) (tetrahedral site)	1	0.323	0.517	−0.60	–
hcp-Zr(H) (octahedral site)	1	0.323	0.517	−0.56	–
fcc-Zr(H) (tetrahedral site)	11	0.323	–	−0.19	–
fcc-Zr(H) (octahedral site)	11	0.322	–	−0.43	–
ζ Hydride	25	0.325	1.078	–	−0.23
γ Hydride	50	0.457	0.501	–	−0.44
δ Hydride [1 0 0]	60	0.475	0.483	–	−0.50
δ Hydride [1 1 0]	60	0.469	0.494	–	−0.51
δ Hydride [1 1 1]	60	0.477	–	–	−0.52
δ Hydride (SQS average)	60	0.478	–	–	−0.53
ε Hydride	66	0.500	0.442	–	−0.59

importance as it represents a reference point for comparison in further calculations. The number reported here of −0.60 eV compares favourably with −0.52 eV from Ref. [38], −0.604 eV from Ref. [12] and −0.464 eV from Ref. [39]. The tetrahedral site for H occupancy remains the most favourable, in agreement with most prior work [12,18,38,39]. For the remainder of this work, when considering sites for H occupancy, only the tetrahedral site is considered. More exotic configurations such as H_2 dimers on interstitial sites have also previously been found to be unfavourable [12].

With regards to the approximate δ phase, $ZrH_{1.5}$, a conventional unit cell of fcc Zr offers eight sites for H occupancy, six of which must be filled with the other two vacant. If the system is cubic, then symmetry reduces the number of configurations to three different arrangements. These arrangements are where the vacancies are both in the [1 0 0], [1 1 0] and [1 1 1] directions. These are referred to in Table 2 by these directions. The configuration with the lowest enthalpy of formation is the one in the [1 1 1] orientation, where the vacancies are separated by the longest distance. The energy difference between these states is relatively small, and similar (but slightly larger) than the average of the energy calculated from using the three SQS configurations.

3.2. Statistical analysis

In order to ensure that the simulations are representative of the disordered system it is important that a large enough sample of the configuration space is achieved. With this in mind, the statistical parameters generated in the sets used are shown in Table 3. The δ and solid-solution series rely on a random distribution about the selected stoichiometry, while the ζ and γ phases use the skew-random method. A large enough sample has been made when the data set forms a normal distribution centred on the target stoichiometry. A simple convention for determining normality is a plot of the cumulative distribution probabilities of the data against theoretical cumulative distribution probabilities generated by a standard normal distribution [40], with the parameters in Table 3. A straight-line fit would represent perfectly normal data. Normality tests were performed on sets of increasing sample size until a high degree of confidence in normality was achieved. Fig. 2(a) and (b) show normality tests for each set of data, generated from both the stoichiometry distribution and the formation enthalpy distribution. In both cases, we see all series display a good linear fit. We report that for sample sizes of 50 cells per set, all datasets showed high coefficients of linear regression with the lowest R^2 being 0.9602. The average stoichiometry for each set is extremely close to the experimental formula value considered representative for that hydride structure. This gives confidence in the hypothesis that this set of randomly generated structures approximates a disordered material when taken as a whole.

Table 3
Statistical values collected from the different data sets used in this work. N is the size of the set, $\sum H$ is the total number of H sites, x^{min}_{stoich} and x^{max}_{stoich} are the lower and upper ranges of the stoichiometry, $\bar{x}_{stoich}$ is the arithmetic mean of the stoichiometry and σ_{stoich} is the standard deviation from the mean.

	N	$\sum H$	x^{min}_{stoich}	x^{max}_{stoich}	$\bar{x}_{stoich}$	σ_{stoich}
Solid solution	50	800	0.13	0.50	0.19	0.08
ζ hydride	50	800	0.44	0.88	0.57	0.09
Randomized γ	15	480	0.63	1.25	1.00	0.16
γ hydride	50	1600	0.75	1.38	1.03	0.18
δ hydride	50	1600	1.25	1.88	1.66	0.16
SQS δ hydride	3	192	1.50	1.75	1.63	0.10

3.3. Enthalpies

Relative thermodynamic phase stability can be determined by plotting the formation energy across the range of compositions, in the form of a convex hull diagram, see Fig. 3. Specifically, this represents a latent formation enthalpy, as opposed to a free energy. Here, a convex hull is defined as the smallest convex path to contain all of the available data points, when viewed from below the plot. It is useful, because any mixture with an enthalpy less negative than the convex hull would be more stable as a mixture of the two configurations which bound that segment of the hull.

In Fig. 3, all enthalpies are negative, indicating that there is a general thermodynamic driving force for formation, which becomes stronger with greater H-content

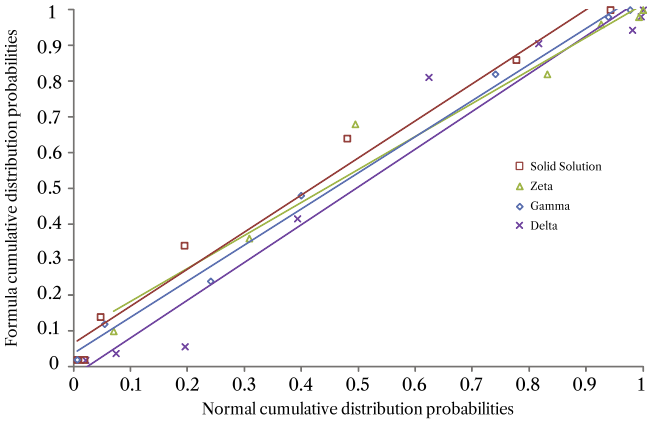

(a) Frequency distribution analysis of the variation of x in ZrH_x.

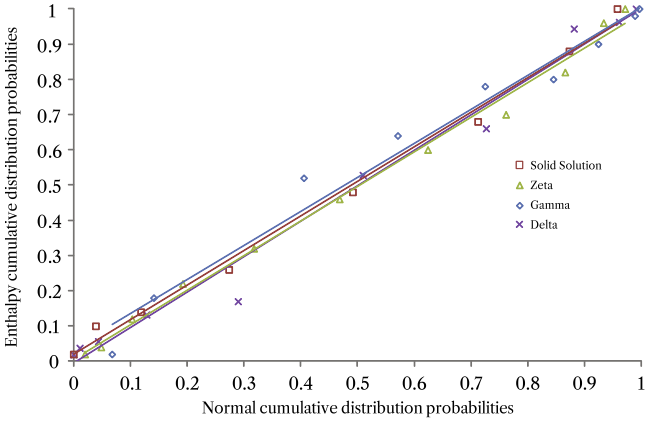

(b) Frequency distribution analysis of formation enthalpies.

Fig. 2. Normality test plots for the structures generated in this study.

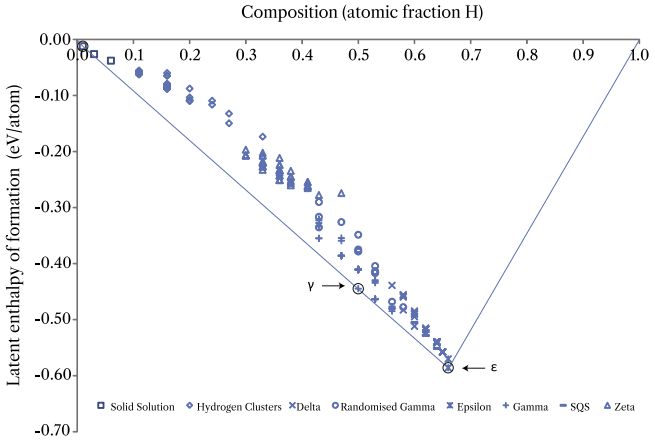

Fig. 3. The normalised latent enthalpy of formation from pure elements for all structures studied in this work. The shape of the marker indicates to which simulation series it belongs. Circled points rest on the convex hull.

phases. However, the majority of configurations lie above the convex hull, indicating they are less stable than a mixture of other phases. The configurations which lie on the convex hull are the 1 at.% H solid solution, the stoichiometric and ordered γ hydride, and the ε phase with a c/a ratio of less than 1. The enthalpies in the stoichiometry range $ZrH_{0.01}$ to $ZrH_{0.6}$ agree with a similar plot produced by Hollinger et al. [41] in terms of the range of formation enthalpies of the different structures. However, whereas that work noted stable structures in this range, none are found in the present work. This is almost certainly due to the fact that the work of Hollinger et al. was focused on hexagonal phases, whereas the present work shows that cubic phases out-compete hexagonal structures in terms of stability. Domain et al. [12] provide a similar plot with no convex hull; however, adding one demonstrates the same phases (ε and γ) as stable and by similar energies. This result has also been found by Zhong and MacDonald [24], who used this data to suggest that the γ phase is thermodynamically stable below $\approx$ 523K. This contrasts greatly with Zhu et al. [13], who claimed that the δ hydride is by far the most stable hydride, by nearly 8 eV more than the other phases. It is, however, difficult to understand that result, since the "convex hull" presented was not actually convex, and the magnitude of this number is out of line with other results [12,24,38,41].

Ultimately, hydrides are formed by the precipitation of H from solid solution in the α-Zr matrix. This reaction is given by the expression:

$$\Delta E^P = \left[E(Zr_xH_y) + (y)E(Zr_R)\right] - \left[yE(Zr_RH) + xE(Zr)\right] \quad (4)$$

Eq. (4) forms the basis of calculating the change in different thermodynamic parameters such as the latent enthalpy of precipitation. The term R is the number of Zr atoms in the solid-solution reference cell. Precipitation enthalpies have been calculated using reference solutions containing 96, 36 or 16 atoms of Zr to one atom of H. This equation is balanced with free Zr on both sides because it ensures that the reaction maintains reversibility in situations where the concentration is different. As with the formation enthalpies, these precipitation enthalpies must be normalised to ensure that larger simulations are not shown as having larger enthalpies purely based on their size, and not on changes in composition and thermodynamic behaviour. To this end, all simulations are divided by the total number of H atoms present in the hydride phase, and then converted into kJ mol^{-1}. Thus, the enthalpies presented henceforth are in units of kJ mol H^{-1}, representing the enthalpy change required for 1 mol of H atoms to precipitate from a solid solution.

The latent enthalpies of precipitation are presented in Fig. 4. As with the formation enthalpies, there is a general trend that the precipitation of H-rich hydrides is more preferable than H-poor hydrides. On the H-poor side of the graph, solid solutions have more negative enthalpies when they are less concentrated than the reference solid solution for that series, suggesting a trend towards dilution of H atoms. Moving across towards products with a greater H content, there is then a peak of unfavourable H clusters around $ZrH_{0.2}$, followed by a steady return to the more preferable hydride phases. In particular, the γ phase exhibits the strongest preference for precipitation, with the most favourable configuration being the structure typically

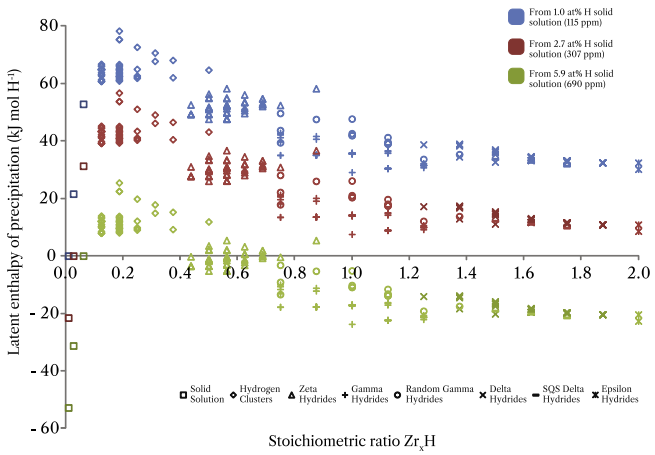

Fig. 4. The normalised latent enthalpy for all structures studied in this work. The shape of the marker indicates to which simulation series it belongs, and the colour indicates the concentration of the initial solid solution. These numbers are normalised with respect to the number of H atoms precipitated.

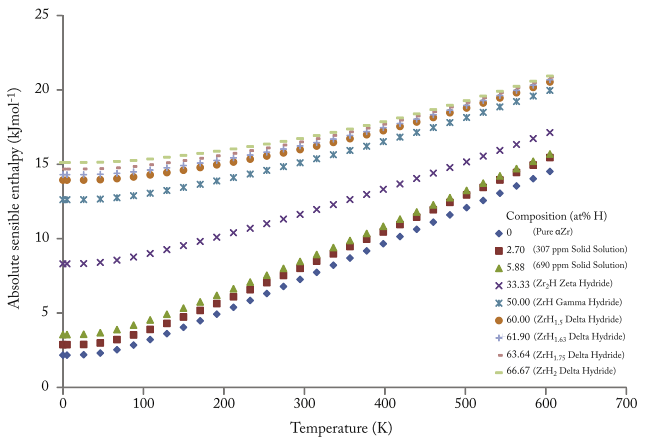

Fig. 5. The absolute sensible enthalpy plotted against temperature for a variety of reference simulations. The temperature–composition–enthalpy surface resulting from this data is used to interpolate sensible enthalpies for further calculations.

modelled in other simulation studies, shown in Fig. 1. There is a notable discontinuity in all series at $\approx ZrH_{0.75}$, corresponding to the point where the series switched from modelling hcp hydrides to fcc hydrides.

There are no negative latent enthalpies of precipitation for the precipitations from 1 at.% H and 2.7 at.% H solid solutions. However, there are for the 5.9 at.% H solid solution. It is sensible that increasing the H content in the Zr lattice increases the impetus for the rearrangement of the H atoms into a hydride, as is evidenced by the existence of a terminal solubility limit for H in Zr [2]. Overall, this plot is consistent with H having a bimodal distribution in Zr, preferring to exist either as a sparsely distributed solid solution, or as a concentrated hydride. A middle ground between these two modes is unfavourable.

So far, this only describes the latent enthalpy with no regards for the effects of temperature. The sensible enthalpy of precipitation is related to the heat capacities of the products and reactants of the precipitation reaction. Heat capacities calculated at 298 K are 23.00 kJ mol^{-1} K^{-1} for α-Zr and 28.64 kJ mol^{-1} K^{-1} for ε-ZrH_2 (compared with the available experimental values of 25.45 kJ mol^{-1} K^{-1} and 31.08 kJ $mol^{-1}K^{-1}$ [42]). Fig. 5 gives the absolute sensible enthalpies for reference simulations, as these vary with temperature. The values for the three δ phase stoichiometries are calculated using the SQS-generated cells. There is a general trend for increasing sensible enthalpy with increasing H content. The ζ phase has a substantially lower sensible enthalpy than the other hydride phases. As the temperature increases, the variance in sensible enthalpies decreases. The enthalpy calculated at 0 K represents the zero point energy contribution to the enthalpy of this system.

The absolute sensible enthalpy is of less interest than the change in sensible enthalpy which may drive precipitation. Using Fig. 5, a surface is generated to describe the relationship between composition, temperature and sensible

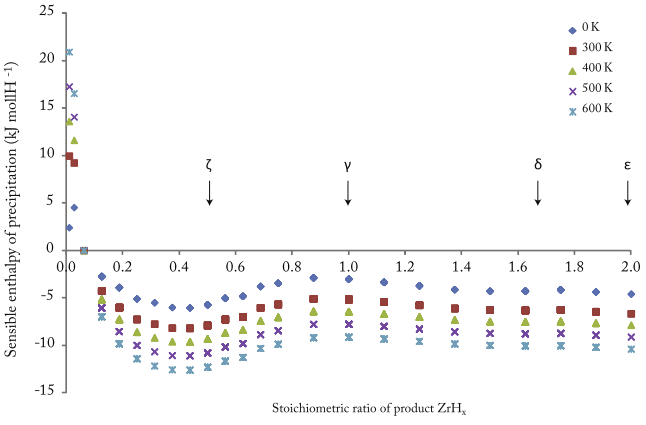

Fig. 6. The sensible enthalpy change during precipitation as a function of stoichiometry. These numbers are normalised with respect to the number of H atoms precipitated.

enthalpy. Using this surface, values are interpolated for sensible enthalpies for all the cells examined in this work. The enthalpy data is sufficiently close that a simple linear interpolation does not introduce unreasonable variance. Feeding this interpolation into Eq. (4), the sensible enthalpy change during precipitation for a variety of different structures and temperatures is generated and plotted in Fig. 6. This information is presented only for the precipitation from the 16 atom solid solution. Given that the sensible enthalpy is added to the latent enthalpy, in Eq. (1), a negative value of sensible enthalpy represents a driving force for precipitation, while a positive value represents a driving force for solution. The sensible enthalpy appears to drive the system towards precipitation for all product stoichiometries greater than $\sim ZrH_{0.08}$. As temperature increases, the driving force for precipitation also increases. There is a relative increase in this driving force for stoichiometries of $\sim ZrH_{0.4}$, which corresponds roughly with the

stoichiometries found in the ζ phase hydrides. The sensible enthalpy then becomes less negative for stoichiometries appropriate to γ hydrides before reducing slightly for hydrides with even greater H content.

3.4. Entropy

As described previously, computing the free energy of a reaction requires a description of the entropy as well as the enthalpy. In this study, we examine two sources of entropy—the vibrational and the configurational.

Configurational entropy stems from the disorder available when the structure may have multiple different forms. It is quantified by the Boltzmann entropy equation:

$$S_c = k \ln \Omega \tag{5}$$

where Ω is defined as the number of different configurations or microstates in which the system may be arranged and k is Boltzmann's constant. In an atomistic context, the number of different structure configurations is given by adopting the standard permutation expression:

$$\Omega = \frac{(N_V + N_H)!}{N_V! N_H!} \tag{6}$$

where N_V is the number of potential H sites that are vacant, while N_H is the number of H atoms.

As before, the primary concern is not the absolute entropy, but the change in entropy during precipitation. Using the entropy calculated from Eq. (5) in the precipitation Eq. (4) (with the H coming from the 16 atom Zr cell), the change in configurational entropy is determined across a range of stoichiometries, and displayed in Fig. 7. These entropies are presented as a $T\Delta S$ product. As entropies are subtracted from enthalpies to generate a free energy, a negative value indicates a driving force towards solution, while a positive value drives towards precipitation. For non-zero temperatures, we see that the configurational entropy represents a driving force for solution, which, of course, increases with increasing temperature. There is a notable discontinuity when the simulated series shift to modelling fcc hydrides. This is because the fcc structure has more tetrahedral sites per Zr atom, which are considered as possible sites for H occupancy (i.e. it offers greater configurational options). Thus, the shift from hcp to fcc is favoured by the configurational entropy and this driving force increases with temperature.

The final contribution examined in this work is the vibrational entropy. Vibrational entropies are shown in Fig. 8 for the same reference cells as used to calculate the sensible enthalpy. Vibrational entropies at 298 K are 37.52 J mol^{-1} K^{-1} for α-Zr and 31.387 J mol^{-1} K^{-1} for ε ZrH_2, compared with the available experimental values of 39.144 and 35.154 J mol^{-1} K^{-1}, respectively [42]. It should be noted that the experimental results will include other forms of entropy (such as that generated by intrinsic defects on the Zr lattice), hence it is reasonable that the theoretical results are slightly smaller than the experimental values. Fig. 8 demonstrates a decreasing vibrational entropy with increasing H content. Similar to the calculation of sensible enthalpies, this plot is used to interpolate values from a temperature–composition–entropy surface. Applied across the range of compositions, the vibrational entropy is given in Fig. 9 as a $T\Delta S$ product. This plot shows negative values for all compositions above $\sim ZrH_{0.08}$, and temperatures above 0 K. This is consistent with the vibrational entropy driving the reaction towards solution, with the effect becoming stronger with increasing temperature. The vibrational entropy change during precipitation is positive for dilute solid solutions, becomes negative for non-dilute solutions, and becomes more negative as H content increases. There is a decrease in the magnitude of the entropy change for hydrides of around $\sim ZrH_{1.5}$, suggesting vibrational entropy may contribute to stabilizing the δ phase.

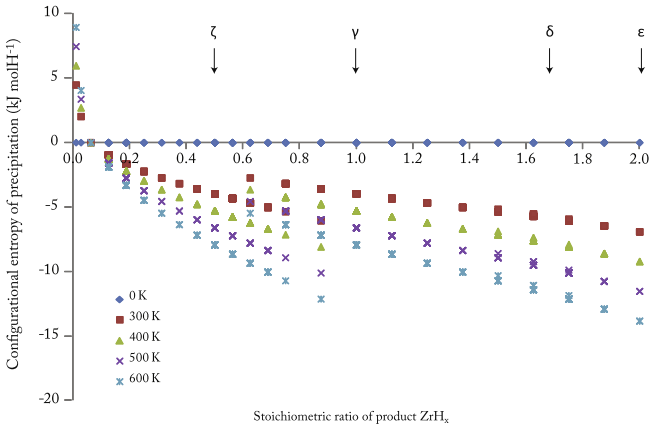

Fig. 7. The configurational entropy change during precipitation as a function of stoichiometry. These numbers are normalised with respect to the number of H atoms precipitated. It should be noted that these are presented as a $T\Delta S$ product.

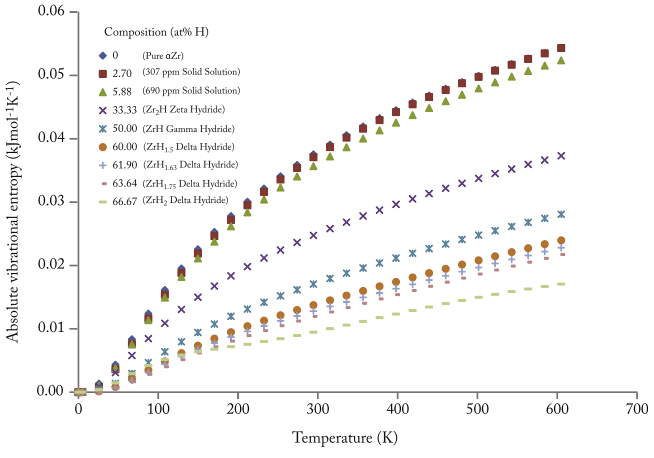

Fig. 8. The absolute vibrational entropy plotted against temperature for a variety of reference cells. The temperature–composition–entropy surface resulting from this data is used to interpolate vibrational entropies for further calculations.

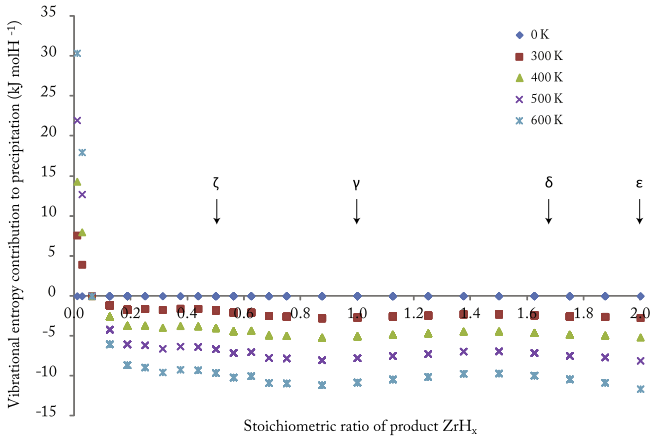

Fig. 9. The vibrational entropy change during precipitation as a function of stoichiometry. These numbers are normalised with respect to the number of H atoms precipitated. It should be noted that these are presented as a $T\Delta S$ product.

3.5. Free energy

With the change in both the enthalpy and entropy terms calculated for the precipitation reaction, the overall free energy change can be calculated from Eq. (2). It is sometimes stated that vibrational entropies and sensible enthalpies are too small to be important in this system and other hexagonal metals [43]. Although this may be true for predicting if hydrides occur at all, and for determining energies when one reactant is in a different state (e.g. H_2 gas), in a system with multiple solid phases, containing subtle interactions, the magnitude of these other terms may be important. Given that the sensible enthalpy and configurational and vibrational entropy terms (as $T\Delta S$ products) are all within the range of −20 to 40 kJ mol H^{-1}, none of these variables can be discounted and all have a part to play in determining phase stability.

In Fig. 10(a)–(c), the lowest energy configuration from each data set is plotted as a free energy, with respect to the stoichiometry. Fig. 10(a) represents the free energy of precipitation from the 96 atom cell, Fig. 10(b), is from the 36 atom cell, and Fig. 10(c) is from the 16 atom cell. In the first of these plots, Fig. 10(a), the free energy remains positive across the entire stoichiometry range. Temperature raises the energy by over three times the 0 K values. As with all these plots, there appear to be five distinct regions, defined by stoichiometry. The first occurs between $ZrH_0 \rightarrow ZrH_{0.1}$. Here, increasing the stoichiometry drastically increases the free energy of precipitation, suggesting that concentrating the H in the lattice is energetically unfavourable. This reaches a relatively flat region 2, made up of clusters of H atoms. This is particularly unfavourable, suggesting that H prefers to remain distributed. There is then a significant drop in free energy entering into region 3. The start of region 3 contains both H clusters, and sub-stoichiometric ζ hydrides as modelled by the skew-random technique. The ζ hydrides are more energetically favourable, and have a minimum energy point at $ZrH_{0.5}$, for the

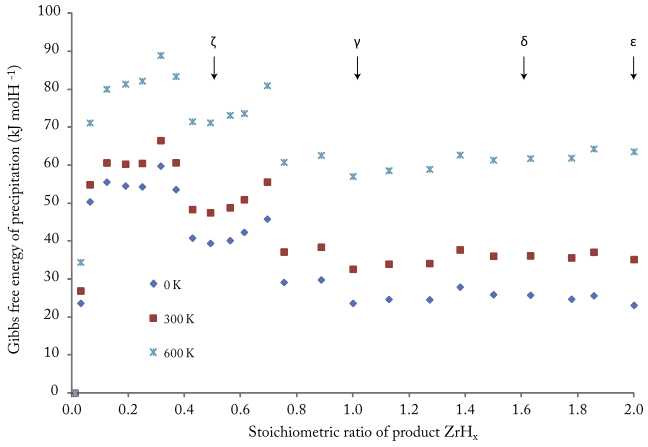

(a) Precipitation from a 1.0 at%H solid solution.

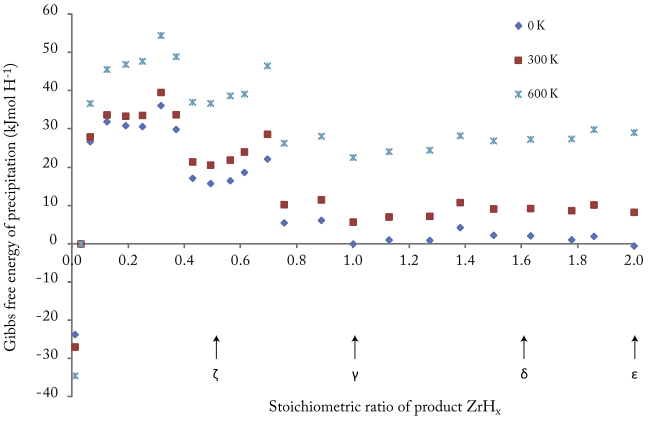

(b) Precipitation from a 2.7 at%H solid solution.

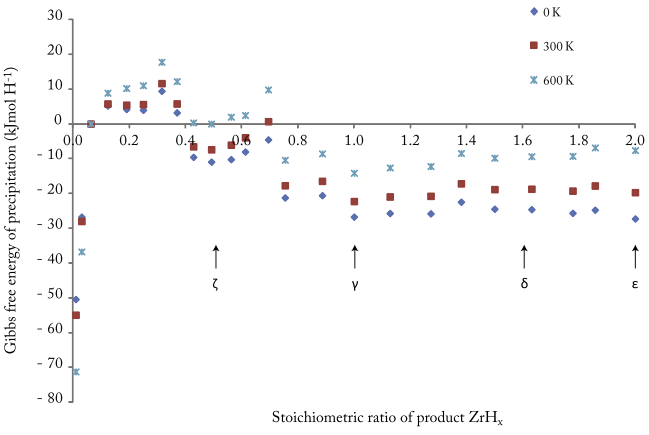

(c) Precipitation from a 5.9 at%H solid solution.

Fig. 10. The final Gibbs free energy of precipitation, as a function of stoichiometry, from different starting concentrations. These numbers are normalised with respect to the number of H atoms precipitated.

expected structure of the ζ hydrides. However, as H content continues to increase, the free energy rises again and is out-competed by the sub-stoichiometric γ phase at the start of region 4. This phase remains competitive until region 5 is entered, where stoichiometries are closer to that of the δ phase than γ. Beyond this, energies remain

relatively flat until the terminating ε phase is reached. As temperatures increase, region 5 begins to show a slight upwards slope, signifying it is more preferable to precipitate larger quantities of H-poor hydrides, than smaller quantities of H-rich hydrides.

Assuming an initial concentration of 2.7 at.% H, see Fig. 10(b), the results are similar to those for 1.0 at.% H; however, the precipitation energies for the γ and ε phases are now just about zero or marginally negative at 0 K. At higher temperatures, precipitation of all the hydrides remains unfavourable, and the reaction is still driven towards solid solution. The free energies are lower overall, and the difference brought about by increasing temperature is smaller.

Finally, the free energies drop significantly when moving to an initial concentration of 5.9 at.% H. Fig. 10(c) shows negative precipitation energies across the full range of stoichiometry and temperatures, with the exception of stoichiometries in the range of $ZrH_{0.1}$ to $ZrH_{0.4}$ (region 2). Below this, there is still a thermodynamic driving force to keep H dispersed, but above this, there is impetus for hydride formation. As in all prior plots, increasing temperature causes free energies to become more positive and drives solution. At the higher temperatures, the energy of the ζ phase increases to the point where its precipitation is no longer thermodynamically favourable. The tendency for regions 4 and 5 to slope upwards at higher temperatures is even greater when precipitation occurs from a more concentrated initial solution. The most favourable phases are γ and ε, although higher temperatures seem to favour γ hydrides. Overall, this remains consistent with a bimodal H distribution, as described previously.

4. Discussion

4.1. Hydrogen in zirconium

It is well established that there is a strong thermodynamic impetus for H to become sequestrated in a Zr lattice. This is corroborated by the energy values given for H solution in Table 2, which are all substantially negative. If we compare this for any of the values for precipitation, we see that the impetus of adding H to the Zr lattice is substantially greater than the energy of rearranging or precipitating the H once it is already in the lattice. This means that if the thermodynamic values for H_2 gas are less affected by temperature than the solid solution values are, it would be expected that H will continue to be added to Zr over the life of the cladding, steadily driving up the H concentration.

In Fig. 10(a) and (b), the lowest free-energy configuration is the 1.0 at.% H solid solution, suggesting that H will preferentially form a dilute solid solution if possible. Temperature effects drive this behaviour further, in that the energy of the 1.0 at.% H solid solution becomes more negative and the more H-rich solid solutions become more positive. In order to produce this behaviour, there must be some sort of interaction between H atoms that raises the energy of the system. Given that electron interactions have been previously demonstrated to be extremely localised to H atoms in the H–Zr system [12], it is unlikely that the chemistry of H is driving this response. This leaves geometrical factors and most notably stress. It is possible that the stress fields created by the insertion of H atoms into nearby interstitial positions in the Zr lattice are mutually repulsive.

4.2. Implications for hydride precipitation

If there is an initial impetus for H atoms to remain in solid solution, then given that hydrides have been noted to form experimentally, at some point conditions must change to favour hydride formation. As more and more H atoms are absorbed by the Zr, the barrier for H atoms to congregate must be overcome. In Fig. 10(c), a high starting concentration of 5.9 at.% H provides this condition. This suggests that at some point between 307 and 690 ppm H atoms will be so numerous that they will be pushed past their mutually repulsive behaviour and will start to form hydrides. These values are significantly higher than those measured globally in actual alloys, implying Zr has a much higher local H carrying capacity than suggested experimentally [44]. If this is the case, in order for precipitation to occur, forces beyond those predicted in these DFT simulations must generate a driving force for concentration, and hence precipitation. Given this case, it is possible that larger-scale stress states, such as those provided by defects or cracks, could lessen this mutually repulsive force, allowing H atoms to diffuse together more easily. The idea that stress impacts diffusion is not new, and has been suggested as a key part of the mechanism behind delayed hydride cracking [1,44,45]. It is reasonable that the Zr lattice around an interstitial H atom is in a state of compression. Given this, a tensile stress field would provide a nullifying effect on the repulsive interaction. Coupled with areas that are not under stress, there would be an impetus for H atoms to move away from regions where H atoms are in close proximity and not under tension, towards areas where they can congregate more favourably. This argument is based upon the existence of the aforementioned barrier to association, and provides an area which can be investigated in future studies.

Temperature also has the effect of driving the system towards solution, by raising the composition of the first point at which hydriding may occur. In the room temperature series (300 K), the first hydride with a negative free energy of precipitation has a composition of about $ZrH_{0.43}$, while in the operating temperature series, this is raised to over $ZrH_{0.7}$. The main reason for this increase is entropic, in that both the configurational and vibrational entropy drive the reaction towards solution.

4.3. Zirconium hydrides

The free energy curves produced in this study can be used to predict which hydride phase will precipitate, should

precipitation occur. At 0 K, The γ, δ and ε hydrides present similar formation energies, suggesting that thermodynamically they may coexist at equilibrium, as observed experimentally [4,46,47], if other factors such as local stress and interfacial energy are disregarded. On the other hand, the ζ phase presents significantly less favourable formation energy compared to the other hydrides, yet a local minima is found in the free energy curve about the $ZrH_{0.5}$ composition, suggesting that the ζ hydride may be metastable, in agreement with previous work [11]. Fig. 10(c) indicates that as temperature increases, the stability of the γ phase relative to ε increases. The primary driver of this is the configurational entropy. Thus, in a reactor, we would expect to see γ phase hydrides, while at room temperature or lower, hydrides with a greater H content are favoured. This is in accord with the experimental observation that γ phase hydrides have been observed to form primarily in rapidly cooled samples [16,48,49], but samples with a relatively low H content allowed the formation of γ hydrides under slower cooling [6,10,14]. There are, however, other factors in the precipitation of hydrides that are difficult to investigate using DFT, such as stress states caused by the anisotropic expansion of α-Zr grains and by the nucleation and growth of the hydrides themselves [4,17], the formation of Zr–hydride interfaces [46] and the effect of matrix hardening [14,50–52]. Given the small differences in free energy between the γ, δ and ε hydride phases reported in the current work, it is expected that these factors may play an important role in the thermodynamics of hydride precipitation, dictating which phase is favoured over others [16,49] or whether they may coexist in the same sample [4,15,34].

5. Conclusion

This work has used DFT to investigate the thermodynamics of the precipitation of Zr hydrides over a range of temperatures, compositions and starting solid-solution concentrations. The use of statistically significant numbers of randomly generated configurations has been coupled with SQS cells to ensure that disordered cells are modelled accurately. This investigation has led to the following conclusions:

- H favours a bimodal distribution within the Zr lattice. At low concentration, H prefers to maintain a dilute, non-clustered configuration, with a high energy barrier to hydride formation. As more H is absorbed by the Zr, this barrier is overcome and hydride precipitation becomes energetically favourable.
- The predicted concentration of the H solutions required to initiate precipitation is greater than observed experimentally, suggesting additional mechanisms may be needed to enhance local H concentration to drive precipitation. Stress may play a part in this.
- The calculation of latent enthalpies alone is insufficient to fully describe this system. Vibrational entropy, configurational entropy and sensible enthalpy are important for dealing with the phase stabilities of precipitates and solid solutions.
- Sensible enthalpies drive the reaction towards precipitation and are particularly significant for the ζ hydride.
- Configurational entropy drives the system towards solution, and is particularly significant when contemplating the difference between hcp- and fcc-based hydrides.
- Vibrational entropy and thus temperature drives the system towards solution.
- Generally, the γ phase is the most stable, suggesting other mechanisms (e.g. precipitate interface lattice strain) may be responsible for the observed presence of δ hydrides.

Acknowledgements

Special thanks go to M.J.D. Rushton for his generous assistance. S.C.L. and M.R.W. acknowledge financial support from the MoD from a UDS Grant. M.R.W. acknowledges support from EDF Energy through an industrial Fellowship award. S.T.M. and P.A.B. acknowledge financial support through an EPSRC Grant (EP/I003320/1) and ANSTO, respectively. All authors acknowledge the use of Imperial College's high-performance computing centre.

References

[1] Puls MP. The effect of hydrogen and hydrides on the integrity of zirconium alloy components: delayed hydride cracking. Berlin: Springer; 2012.
[2] Kearns JJ. Atom Eng 1967;22:292–303.
[3] Kearns JJ. J Nucl Mater 1972;43:330–8.
[4] Barrow ATW, Toffolon-Masclet C, Almer J, Daymond MR. J Nucl Mater 2013;43:395–401.
[5] Mallett MW, Albrecht WM. J Electrochem Soc 1957;104(3):142.
[6] Ells E. J Nucl Mater 1968;28:129–51.
[7] Raynauld P, Bielen A. Cladding hydrogen based regulations in the United States. Water reactor fuel performance meeting. Chengdu, China; 2011.
[8] Kessler J, Einziger R. Technical bases for extended dry storage of spent nuclear fuel. Palo Alto, CA: EPRI; 2002.
[9] Okamoto H. J Phase Equilib Differ 2006;27(5):548–9.
[10] Weatherly GC. Acta Metall 1981;29(3):501–12.
[11] Zhao Z, Morniroli JP, Legris A, Ambard A, Khin Y, Legras L, et al. J Microsc 2008;232(3):410–21.
[12] Domain C, Besson R, Legris A. Acta Mater 2002;50(13):3513–26.
[13] Zhu W, Wang R, Shu G, Wu P, Xiao H. J Phys Chem C 2010;114(50):22361–8.
[14] Lanzani L, Ruch M. J Nucl Mater 2004;324(2–3):165–76.
[15] Root JH, Fong RWL. J Nucl Mater 1996;232:75–85.
[16] Nath B, Lorimer GW, Ridley N. J Nucl Mater 1975;58:153–62.
[17] Steuwer A, Santisteban J, Preuss M, Peel M, Buslaps T, Harada M. Acta Mater 2009;57(1):145–52.
[18] Burr PA, Murphy ST, Lumley SC, Wenman MR, Grimes RW. Corros Sci 2013;69:1–4.
[19] Fukai Y. The metal–hydrogen system. Berlin: Springer Verlag; 1993.
[20] Glazoff MV, Modeling of some physical properties of zirconium alloys for nuclear applications in support of UFD campaign. Technical Report, Idaho National Laboratory; 2013.
[21] Glazoff MV, Tokuhiro A, Rashkeev SN, Sabharwall P. J Nucl Mater 2014;444(1-3):65–75.
[22] Ackland G. Phys Rev Lett 1998;80(10):2233–6.

[23] Blomqvist J, Olofsson J, Alvarez A, Bjerk C, Structural and thermodynamical properties of zirconium hydrides from first principles. in: 15th international conference on environmental degradation of materials in nuclear power systems-water reactors; 2012.
[24] Zhong Y, MacDonald DD. J Nucl Mater 2012;423:87–92.
[25] Zunger A, Wei S, Ferreira LG, Bernard JE. Phys Rev 1990;65(3):353–6.
[26] Wang H, Chroneos A, Jiang C, Schwingenschlögl U. Phys Chem Chem Phys 2013;15(20):7599–603.
[27] Mao Z, Seidman DN, Wolverton C. APL Mater 2013;1:042103.
[28] Akbarzadeh AR, Wolverton C, Ozolins V. Phys Rev B 2009;79:184102.
[29] Clark SJ, Segall MD, Pickard CJ, Hasnip PJ, Probert MJ, Refson K, et al. Z Kristallogr 2005;220:567–70.
[30] Vanderbilt D. Phys Rev B 1990;41(11):7892–5.
[31] Monkhorst H, Pack J. Phys Rev B 1976;13(12):5188–92.
[32] Methfessel M, Paxton A. Phys Rev B 1989;40(6):3616–21.
[33] Pfrommer BG, Cote M, Louie GS, Cohen ML. J Comput Phys 1997;131:133–40.
[34] Barrow ATW, Korinek A, Daymond MR. J Nucl Mater 2013;432(1–):366–70.
[35] Baroni S, de Gironcoli S, Corso A. Rev Mod Phys 2001;73(2):515–62.
[36] Frank W, Elsässer C, Fähnle M. Phys Rev Lett 1995;74(10):1791–4.
[37] Pickard CJ, Needs RJ. J Phys Cond Mat 2011;23(5):053201.
[38] Udagawa Y, Yamaguchi M, Abe H, Sekimura N, Fuketa T. Acta Mater 2010;58(11):3927–38.
[39] Burr PA, Murphy ST, Lumley SC, Wenman MR, Grimes RW. J Nucl Mater 2013;443(1):502–6.
[40] Chambers J, Cleveland W, Kleiner B, Tukey P, Graphical methods for data analysis, Wadsworth; 1983.
[41] Holliger L, Legris A, Besson R. Phys Rev B 2009;80(9):1–9.
[42] Lide DR. Handbook of chemistry and physics. 80th ed. Boca Raton, FL: CRC Press; 1999.
[43] Nicholson KM, Sholl DS. Phys Rev B 2012;86:134113.
[44] McRae GA, Coleman CE, Leitch BW. J Nucl Mater 2009;396:130–43.
[45] Puls MP. J Nucl Mater 2009;393(2):350–67.
[46] Barraclough K, Beevers C. J Nucl Mater 1970;34:125–34.
[47] Veleva M, Arsene S, Record M, Bechade JL, Bai J. Metall Mater Trans A 2003;34:567–78 (March).
[48] Bradbrook J, Lorimer G, Ridley N. J Nucl Mater 1972;42:142–60.
[49] Northwood DO. J Less Common Met 1976;48(1):173–5.
[50] Cann CD, Puls MP, Sexton EE, Hutchings WG. J Nucl Mater 1984;126(3):197–205.
[51] Perovic V, Weatherly G. Acta Metall Mater 1992;40(2):363–72.
[52] Tulk E, Kerr M, Daymond MR. J Nucl Mater 2012;425(1–3):93–104.
[53] Goldak J, Lloyd LT, Barrett CS. Phys Rev 1966;144(2):480–4.
[54] McQuarrie DA, Simon JD. Physical chemistry: a molecular approach. 1st ed. University Science Books; 1997.